Chinese Journal of Aeronautics, (2016), xxx(xx): xxx–xxx

Chinese Society of Aeronautics and Astronautics
& Beihang University

Chinese Journal of Aeronautics

cja@buaa.edu.cn
www.sciencedirect.com

REVIEW ARTICLE

Flight safety measurements of UAVs in congested airspace

Xiang Jinwu, Liu Yang, Luo Zhangping *

School of Aeronautic Science and Engineering, Beihang University, Beijing 100083, China

Received 2 September 2015; revised 18 November 2015; accepted 15 June 2016

KEYWORDS

Airspace safety situation;
Conflict probability;
Flight conflict;
Navigation;
UAV

Abstract Describing spatial safety status is crucial for high-density air traffic involving multiple unmanned aerial vehicles (UAVs) in a complex environment. A probabilistic approach is proposed to measure safety situation in congested airspace. The occupancy distribution of the airspace is represented with conflict probability between spatial positions and UAV. The concept of a safety envelope related to flight performance and response time is presented first instead of the conventional fixed-size protected zones around aircraft. Consequently, the conflict probability is performance-dependent, and effects of various UAVs on safety can be distinguished. The uncertainty of a UAV future position is explicitly accounted for as Brownian motion. An analytic approximate algorithm for the conflict probability is developed to decrease the computational consumption. The relationship between safety and flight performance are discussed for different response times and prediction intervals. To illustrate the applications of the approach, an experiment of three UAVs in formation flight is performed. In addition, an example of trajectory planning is simulated for one UAV flying over airspace where five UAVs exist. The validation of the approach shows its potential in guaranteeing flight safety in highly dynamic environment.

1. Introduction

With increasing numbers of unmanned aerial vehicles (UAVs) and expanded operations into complex mission scenarios, aviation safety is facing a new challenge caused by high-density air traffic in limited airspace. Emergency rescue and formation flying usually suffers in congested airspace. The same problem is encountered by civil aviation when reducing flight separation to improve transportation efficiency and increase airspace capacity, and also by certain innovative techniques under development, such as autonomous risk avoidance and free flight. In order to accomplish complicated military missions safely and effectively, coordinated formation flight (CFF) has been investigated by many researchers. The increase of collision risk among UAVs results in flight safety problems more serious than ever.[1] Fundamentally, an intuitive representation of airspace safety and, especially its tendencies are crucial to

* Corresponding author.
E-mail addresses: xiangjw@buaa.edu.cn (X. Jinwu), youngka@126.com (L. Yang), luozp@buaa.edu.cn (L. Zhangping).

Peer review under responsibility of Editorial Committee of CJA.

ELSEVIER Production and hosting by Elsevier

http://dx.doi.org/10.1016/j.cja.2016.08.017

solving this issue. This leads to the requirement for timely and credible constructs of safety in congested airspace.

The complexity of air traffic dense flight lies in environmental dynamics; therefore, the airspace situation varies dynamically. There are often many maneuvers in low altitude flight, especially for UAVs, and the highly dynamic motions result in difficulty for risk assessment of flight routes. In civil aviation, reliable risk assessment approaches for fixed routes have been developed by Reich[2–4] and Brooker.[5] These methods employed historical statistics to assess the long-term longitudinal, lateral and vertical conflict risks. Assessing airspace complexity in a mid-term horizon has recently attracted more research interest since timely identification of dangerous encounters requiring evasive maneuvers can lead to more efficient ATC system operations.[6] Sridhar et al. describe airspace complexity by the predicted dynamic density.[7] Prandini et al. present an analytic model of air traffic complexity in three dimensional airspace.[8] Due to the presence of flight errors, approaches to evaluate conflict probability involve predicting future aircraft trajectories and computing the probability that two aircraft get closer than a minimum required separation based on these trajectories.[9–13] Usual methods focus on mid-term conflict prediction via the geometric analysis of aircraft relative position. The Monte Carlo approach is a popular method for conflict resolution in the presence of uncertainty in aircraft dynamics,[14–16] though it takes a great amount of computation. Nevertheless, these methods are a posteriori and not appropriate for dynamic and congested airspace. In this work, the occupancy distribution of the airspace, which is represented with conflict probability between spatial positions and UAVs, is proposed as the determinant of airspace safety. In this way, one can have explicit awareness about airspace congestion for a predicted time interval.

In maneuvering flight, aircraft need to frequently perform conflict prediction and resolution; at present, flight routes are varied, and separation minima is difficult to maintain. In conflict prediction, aircraft may encounter intruders from any direction, thus the minimal safe separation is replaced by a protected zone around aircraft (the REICH model is actually a cuboid protected zone). Due to the different kinetic characteristics and flight performance between various types of aircraft, the prescribed protected zone for conflict prediction should relate to aircraft performance. Some research methods, such as the computation of reachable sets, have been developed for this issue. The mathematical formulation of protected zones is generally related to the reachability analysis of aircraft dynamic systems. The analysis attempts to divide the airspace into two parts: those that are reachable from the initial conditions and those that are not. Recently, some contributions have dealt with the mathematical description of reachable sets and their numerical computation.[17–21] Considering that the encounter model is key for assessing conflict probability, we present the safety envelope as the protected zone that should not be penetrated by intruders. It indicates the maximum range that a UAV could reach in a specified response time, then relates the UAV performance to conflict probability.

The rest of the paper is organized as follows: in Section 2, the definitions of UAV safety envelope and airspace safety are introduced; a probabilistic approach for the measure of airspace safety is presented. In Section 3, we analyze the effect of UAV flight performance on conflict probability and construct the airspace safety field. In Section 4, two applications based on airspace safety are presented. In Section 5, conclusions are drawn.

2. Airspace safety

2.1. UAV safety envelope model

The safety envelope is used to characterize the space range that a UAV can reach in a certain time frame. It is an enclosed space determined by UAV flight performance and prescribed time frame. In Fig. 1, the six axes *a, b, c, d, e, f* represent the maximum range that UAV A is able to reach in each direction during the time frame $[0,\tau]$. The safety envelope $E(\boldsymbol{X}^A)$ is composed of eight different one-eighth ellipsoids. The axes e and f are equal due to the bilateral symmetry of UAV flight performance. However, axes a, b, c and d are different. The specified response time is denoted as τ, and V_{f}, V_{b}, V_{a}, V_{d}, V_{l} are the maximum forward velocity, the maximum backward velocity, the maximum vertical ascending velocity, the maximum vertical descending velocity and the maximum horizontal lateral velocity of a UAV, respectively. Hence, we have the maximum range in each direction

$$\begin{cases} a = V_{\mathrm{f}} \times \tau \\ b = V_b \times \tau \\ c = V_{\mathrm{a}} \times \tau \\ d = V_{\mathrm{d}} \times \tau \\ e = f = V_{\mathrm{l}} \times \tau \end{cases} \tag{1}$$

In the inertia coordinate system $\boldsymbol{O}$-xyz (see Fig. 1), for UAV A whose position is $\boldsymbol{X}^A = [x^A, y^A, z^A]^{\mathrm{T}}$, we define the safety envelope $E(\boldsymbol{X}^A)$ as the region centered at $\boldsymbol{X}^A$

$$E(\boldsymbol{X}^A) = \begin{cases} \boldsymbol{X} \in \mathbf{R}^3 | (\boldsymbol{X} - \boldsymbol{X}^A)^{\mathrm{T}} \boldsymbol{M}_1 (\boldsymbol{X} - \boldsymbol{X}^A) \leqslant 1 & x \geqslant x^A, \quad z \geqslant z^A \\ \boldsymbol{X} \in \mathbf{R}^3 | (\boldsymbol{X} - \boldsymbol{X}^A)^{\mathrm{T}} \boldsymbol{M}_2 (\boldsymbol{X} - \boldsymbol{X}^A) \leqslant 1 & x \geqslant x^A, \quad z < z^A \\ \boldsymbol{X} \in \mathbf{R}^3 | (\boldsymbol{X} - \boldsymbol{X}^A)^{\mathrm{T}} \boldsymbol{M}_3 (\boldsymbol{X} - \boldsymbol{X}^A) \leqslant 1 & x < x^A, \quad z \geqslant z^A \\ \boldsymbol{X} \in \mathbf{R}^3 | (\boldsymbol{X} - \boldsymbol{X}^A)^{\mathrm{T}} \boldsymbol{M}_4 (\boldsymbol{X} - \boldsymbol{X}^A) \leqslant 1 & x < x^A, \quad z < z^A \end{cases} \tag{2}$$

where $\boldsymbol{M}_i \in \mathbf{R}^{3\times 3}$ $(i = 1,2,3,4)$ is a diagonal matrix given by

$$\begin{cases} \boldsymbol{M}_1 = \mathrm{diag}\left(\frac{1}{a^2}, \frac{1}{e^2}, \frac{1}{c^2}\right) \\ \boldsymbol{M}_2 = \mathrm{diag}\left(\frac{1}{a^2}, \frac{1}{e^2}, \frac{1}{d^2}\right) \\ \boldsymbol{M}_3 = \mathrm{diag}\left(\frac{1}{b^2}, \frac{1}{e^2}, \frac{1}{c^2}\right) \\ \boldsymbol{M}_4 = \mathrm{diag}\left(\frac{1}{b^2}, \frac{1}{e^2}, \frac{1}{d^2}\right) \end{cases} \tag{3}$$

and $\boldsymbol{M}$ is a function of $\boldsymbol{M}_1$, $\boldsymbol{M}_2$, $\boldsymbol{M}_3$ and $\boldsymbol{M}_4$

$$\boldsymbol{M} = \begin{cases} \boldsymbol{M}_1 & x \geqslant x^A, \ z \geqslant z^A \\ \boldsymbol{M}_2 & x \geqslant x^A, \ z < z^A \\ \boldsymbol{M}_3 & x < x^A, \ z \geqslant z^A \\ \boldsymbol{M}_4 & x < x^A, \ z < z^A \end{cases} \tag{4}$$

Thus, we can rewrite $E(\boldsymbol{X}_A)$ as

$$E(\boldsymbol{X}^A) = \left\{ \boldsymbol{X} \in \mathbf{R}^3 \middle| (\boldsymbol{X} - \boldsymbol{X}^A)^{\mathrm{T}} \boldsymbol{M} (\boldsymbol{X} - \boldsymbol{X}^A) \leqslant 1 \right\} \tag{5}$$

The safety envelope provides maneuvering space for a UAV. In other words, a UAV can perform any maneuver in the safety envelope during the time frame $[0,\tau]$ without

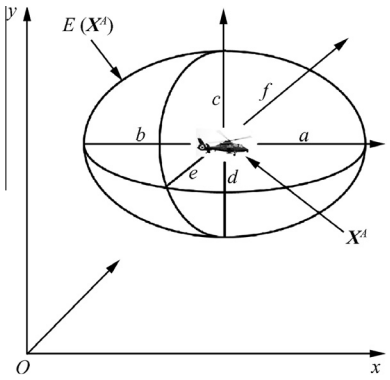

Fig. 1 Safety envelope of UAV A.

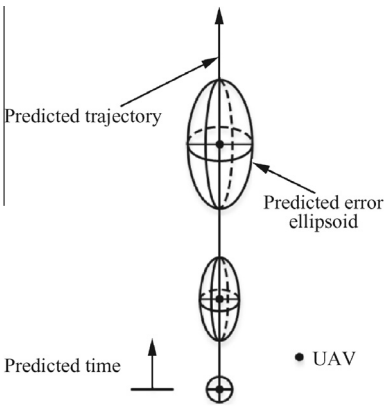

Fig. 2 Future position of a UAV, accounting for uncertainty.

worrying about conflicts with other aircraft. Obviously, the shape of the safety envelope depends on the five velocities that represent UAV flight performance. The parameter τ controls the size of the safety envelope.

2.2. Flight state propagation

Measuring airspace safety involves the estimation of conflict probability, which is only as reliable as the ability of UAV motion model to predict the future. The key to modeling lies in how current UAV states are projected into the future. In the proposed model, future UAV position depends on two elements: the nominal trajectory and uncertainties. Usually, uncertainties are modeled to describe potential variations in the nominal trajectory of a UAV (see Fig. 2).

Suppose UAV A is flying along a nominal trajectory with a velocity profile $\boldsymbol{v}^A$ in the three-dimensional airspace $\boldsymbol{S} \subset \mathbf{R}^3$ during the time horizon $[0, t]$. $\boldsymbol{X}_0^A$ represents UAV initial position at time $t = 0$ s. The UVA's future position is not known precisely due to uncertainty. However, in practice, the prediction error can be modeled through a Gaussian random perturbation whose variance increases both linearly with time t and faster along-track than in the cross-track directions.[7] The UAV predicted position $\boldsymbol{X}^A(t) \in \mathbf{R}^3$ at time t is then formulated by

$$\boldsymbol{X}^A(t) = \boldsymbol{X}_0^A + \int_0^t \boldsymbol{v}^A(s)\,\mathrm{d}s + \boldsymbol{w}^A(t) \quad t \geqslant 0\ \mathrm{s} \tag{6}$$

where $\boldsymbol{w}^A(t) = \boldsymbol{Q}^A(t)\boldsymbol{\Sigma}^A\boldsymbol{B}^A(t)$, with $\boldsymbol{B}^A(t)$ a standard three-dimensional Brownian motion starting from the origin whose variance is given by the matrix $\boldsymbol{Q}^A(t)\boldsymbol{\Sigma}^A \in \mathbf{R}^{3\times3}$.

In detail, $\boldsymbol{\Sigma}^A = \mathrm{diag}(\sigma_1^A, \sigma_2^A, \sigma_3^A)$ is a diagonal matrix whose entries σ_1^A, σ_2^A and σ_3^A are the variance growth rates of the perturbation in the along-track and the two cross-track directions. They comply with the relation $\sigma_1^A \geqslant \sigma_2^A = \sigma_3^A > 0$. $\boldsymbol{Q}^A(t) = [\boldsymbol{q}_1^A(t), \boldsymbol{q}_2^A(t), \boldsymbol{q}_3^A(t)] \in \mathbf{R}^{3\times3}$ is an orthogonal matrix whose first column $\boldsymbol{q}_1^A(t)$ is set as $\boldsymbol{q}_1^A(t) = \boldsymbol{v}^A/\|\boldsymbol{v}^A\|$. Analogous models have been proposed in Refs. 9,11,22 for predicting future aircraft position over tens of minutes.

2.3. Measure of airspace safety

The safety envelope specifies the protected zone of a UAV. If other UAVs enter the safety envelope during the flight time interval $[t_0, t_0 + \Delta t]$, a conflict is considered to have occurred. Similarly, we define the event in which a space point $\boldsymbol{X}$ is in conflict with UAV A as point $\boldsymbol{X}$ entering the safety envelope of UAV A during the time interval $[t_0, t_0 + \Delta t]$. The conflict probability is denoted as

$$p^A(\boldsymbol{X}) = P\{\boldsymbol{X} \in E(\boldsymbol{X}^A) | t \in [t_0, t_0 + \Delta t]\} \tag{7}$$

Assuming multiple UAVs A_i $(i = 1, 2, \ldots, N)$ are flying in the same airspace, the safety of the space point $\boldsymbol{X}$ is denoted as $s(\boldsymbol{X})$. This is the probability that point $\boldsymbol{X}$ is in conflict with at least one UAV during the time interval $[t_0, t_0 + \Delta t]$. It also means that point $\boldsymbol{X}$ enters at least one UAV safety envelope. Then we have

$$s(\boldsymbol{X}) = \bigcup_{i=1}^{N} P(\boldsymbol{X} \in E(\boldsymbol{X}^{A_i}) | t \in [t_0, t_0 + \Delta t]) \tag{8}$$

Note that $s(\boldsymbol{X}) = 0$ means space point $\boldsymbol{X}$ will not be inside any of the existing UAV safety envelopes during the time interval $[t_0, t_0 + \Delta t]$. In addition, $s(\boldsymbol{X}) = 1$ signifies that space point $\boldsymbol{X}$ will enter at least one safety envelope of these UAVs during the time interval $[t_0, t_0 + \Delta t]$. $s(\boldsymbol{X})$ indicates the degree of danger for space point $\boldsymbol{X}$. When $s(\boldsymbol{X})$ exceeds the specified threshold, point $\boldsymbol{X}$ is considered to be dangerous for new UAVs to enter during the time interval $[t_0, t_0 + \Delta t]$.

The probability that space point $\boldsymbol{X}$ enters the safety envelope of UAV A_i during the time interval $[t_0, t_0 + \Delta t]$ is denoted as $p^{A_i}(\boldsymbol{X})$. Assuming the Brownian motion affecting the future positions of these UAVs are independent, the safety situation $s(\boldsymbol{X})$ satisfies

$$s(\boldsymbol{X}) = 1 - \prod_{i=1}^{N}(1 - p^{A_i}(\boldsymbol{X})) \tag{9}$$

The problem of evaluating safety is reduced to that of estimating the conflict probability $p^{A_i}(\boldsymbol{X})$.

2.4. Analysis of conflict probability

Generally, approaches to the calculation of $p^{A_i}(\boldsymbol{X})$ take a great amount of computation. The computing time grows exponentially with the increase in the number of aircraft.[7] Now we will examine an approximate analytical model for the probability $p^{A_i}(\boldsymbol{X})$, dropping the subscript of A_i in the following equations for ease of notation.

The probability $p^A(\boldsymbol{X})$ considers the event where space point $\boldsymbol{X}$ enters the safety envelope $E(\boldsymbol{X}^A)$ centered at $\boldsymbol{X}^A$ with a constant velocity $\boldsymbol{v}^A$ and perturbation $\boldsymbol{w}^A(t)$ during the time interval $[t_0, t_0+\Delta t]$ (see Fig. 3). From the perspective of relative motion, if UAV A is considered to be stationary with only the perturbation $\boldsymbol{w}^A(t)$, then the safety envelope centered at $\boldsymbol{X}$ should move at a constant velocity $-\boldsymbol{v}^A$ contrary to UAV A (see Fig. 4). Hence, $E(\boldsymbol{X}^A)$ and $E(\boldsymbol{X})$ have equal size but different centers. From Eq. (7), we have

$$\begin{aligned} p^A(\boldsymbol{X}) &= P\{\boldsymbol{X} \in E(\boldsymbol{X}^A) | t \in [t_0, t_0+\Delta t]\} \\ &= P\{\boldsymbol{X}^A \in E(\boldsymbol{X}) | t \in [t_0, t_0+\Delta t]\} \end{aligned} \tag{10}$$

With the assumption that UAV A is moving along a straight line of nominal trajectory with constant velocity, Eq. (6) can be rewritten as

$$\boldsymbol{X}^A(t) = \boldsymbol{X}_0^A + \boldsymbol{v}^A t + \boldsymbol{w}^A(t) \quad t \geqslant 0\,\mathrm{s} \tag{11}$$

The relative position $\Delta X(t) = X - \boldsymbol{X}^A(t)$ of UAV A with respect to the point $\boldsymbol{X}$ is given by

$$\Delta \boldsymbol{X}(t) = \boldsymbol{X} - \boldsymbol{X}_0^A - \boldsymbol{v}^A t - \boldsymbol{w}^A(t) \tag{12}$$

Denote $\Delta \boldsymbol{X}_0 = \boldsymbol{X} - \boldsymbol{X}_0^A$ and $\Delta \boldsymbol{v} = -\boldsymbol{v}^A$, Eq. (12) becomes

$$\Delta \boldsymbol{X}(t) = \Delta \boldsymbol{X}_0 + \Delta \boldsymbol{v} t - \boldsymbol{w}^A(t) \tag{13}$$

From Eq. (13), we can consider the motion of UAV A as consisting only of the perturbation $\boldsymbol{w}^A(t)$ and the motion of space point $\boldsymbol{X}$ as determined by constant velocity $\Delta \boldsymbol{v}$ starting from $\Delta \boldsymbol{X}_0$. Then, $p^A(\boldsymbol{X})$ is transformed as the probability that the perturbation $\boldsymbol{w}^A(t)$ hits the safety envelope whose center is moving at a constant velocity for some $t \in [t_0, t_0+\Delta t]$:

$$P\{\boldsymbol{w}^A(t) \in E(\Delta \boldsymbol{X}_0 + \Delta \boldsymbol{v} t) | t \in [t_0, t_0+\Delta t]\} \tag{14}$$

Furthermore, $\boldsymbol{w}^A(t)$ can be transformed to a standard three-dimensional Brownian motion by the following process.

Define the matrix $\boldsymbol{F} = \boldsymbol{Q}^A \boldsymbol{\Sigma}^A$, and the vector $\boldsymbol{\varphi} = \boldsymbol{F}^{-1} \Delta v$. Construct an orthogonal matrix $\boldsymbol{P} = [\boldsymbol{p}_1, \boldsymbol{p}_2, \boldsymbol{p}_3] \in \mathbf{R}^{3\times 3}$ with $\boldsymbol{p}_1 = -\boldsymbol{\varphi}/\|\boldsymbol{\varphi}\|$, then align the first column of $\boldsymbol{P}$ with $-\boldsymbol{\varphi}$. Its inverse $\boldsymbol{P}^{-1} = \boldsymbol{P}^{\mathrm{T}}$ represents a rotation that makes the $-\boldsymbol{\varphi}/\|\boldsymbol{\varphi}\|$ direction coincide with the first coordinate axis direction:

$$\boldsymbol{P}^{-1} \frac{-\boldsymbol{\varphi}}{\|\boldsymbol{\varphi}\|} = \boldsymbol{Z}_1 := [1, 0, 0]^{\mathrm{T}} \tag{15}$$

Using transformation $\Delta \boldsymbol{Z}(t) = \boldsymbol{P}^{-1} \boldsymbol{F}^{-1} \Delta \boldsymbol{X}(t)$, we transform Eq. (13) into

$$\Delta \boldsymbol{Z}(t) = \boldsymbol{r} + \boldsymbol{k} t - \hat{\boldsymbol{B}}(t) \tag{16}$$

where $\hat{\boldsymbol{B}}(t) = \boldsymbol{P}^{-1} \boldsymbol{B}(t)$ is still a standard Brownian motion starting from the origin (rotation of a Brownian motion remains a Brownian motion), and $\boldsymbol{r} \in \boldsymbol{R}^3$, $\boldsymbol{k} \in \boldsymbol{R}^3$ are defined by

$$\begin{cases} \boldsymbol{r} = \boldsymbol{P}^{-1} \boldsymbol{F}^{-1} \Delta \boldsymbol{X}_0 \\ \boldsymbol{k} = \boldsymbol{P}^{-1} \boldsymbol{F}^{-1} \Delta \boldsymbol{v} = \boldsymbol{P}^{-1} \boldsymbol{\varphi} = -\|\boldsymbol{\varphi}\| \boldsymbol{Z}_1 \end{cases} \tag{17}$$

From Eq. (16), we take $p^A(\boldsymbol{X})$ as the probability that the standard Brownian motion $\hat{\boldsymbol{B}}(t)$ starting from the origin hits a moving safety envelope $\hat{E}(\boldsymbol{Z})$ obtained by transforming $E(\Delta \boldsymbol{X}_0 + \Delta \boldsymbol{v} t)$ in the new coordinate system.

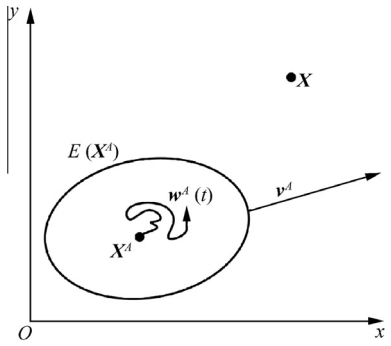

Fig. 3 Probability that $\boldsymbol{X}$ enters $E(\boldsymbol{X}^A)$: $P\{\boldsymbol{X} \in E(\boldsymbol{X}^A) | t \in [t_0, t_0+\Delta t]\}$.

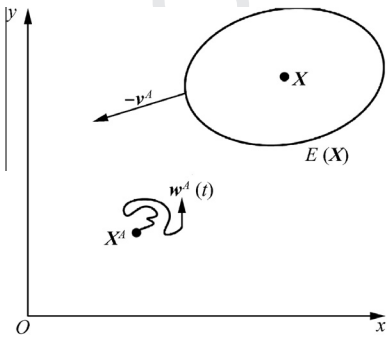

Fig. 4 Probability that $\boldsymbol{X}^A$ enters $E(\boldsymbol{X})$: $P\{\boldsymbol{X}^A \in E(\boldsymbol{X}) | t \in [t_0, t_0+\Delta t]\}$.

$$p^A(\boldsymbol{X}) = P(\hat{\boldsymbol{B}}(t) \in \hat{E}(\boldsymbol{Z}) | t \in [t_0, t_0+\Delta t]) \tag{18}$$

where

$$\hat{E}(\boldsymbol{Z}) = \left\{ \boldsymbol{Z} \in \mathbf{R}^3 \middle| [\boldsymbol{Z} - (\boldsymbol{r} + \boldsymbol{k} t)]^{\mathrm{T}} \boldsymbol{P}^{\mathrm{T}} \boldsymbol{F}^{\mathrm{T}} \cdot \boldsymbol{MFP} [\boldsymbol{Z} - (\boldsymbol{r} + \boldsymbol{k} t)] \leqslant 1 \right\} \tag{19}$$

The center of $\hat{E}(\boldsymbol{Z})$ is moving at the constant velocity $\boldsymbol{k}$ starting from the position $\boldsymbol{r}$. From the construction of matrix $\boldsymbol{P}$, the velocity $\boldsymbol{k}$ is directed along the negative $\boldsymbol{z}_1$ axis (see Fig. 5).

Now the problem of evaluating $p^A(\boldsymbol{X})$ is transformed into a calculation of the probability that the Brownian motion $\hat{\boldsymbol{B}}(t)$ enters the region $\hat{E}(\boldsymbol{Z})$ during the time interval $[t_0, t_0+\Delta t]$.

The probability density function of the three-dimensional standard Brownian motion $\hat{\boldsymbol{B}}(t)$ is

$$f(z_1, z_2, z_3, t) = \frac{1}{(2\pi t)^{\frac{3}{2}}} \mathrm{e}^{-\frac{z_1^2+z_2^2+z_3^2}{2t}} \tag{20}$$

The conflict probability is the integral of the probability density function in the safety envelope $\hat{E}(\boldsymbol{Z})$.

$$p^A(X) = \int_{t_0}^{t_0+\Delta t} \iiint_{\hat{E}(\boldsymbol{Z})} f(z_1, z_2, z_3, t)\, \mathrm{d}z_1\, \mathrm{d}z_2\, \mathrm{d}z_3\, \mathrm{d}t \tag{21}$$

Usually, $\hat{E}(\boldsymbol{Z})$ is an irregular region that results in difficulty calculating the integral Eq. (21). In order to simplify the computation, we use an approximation that replaces the integral

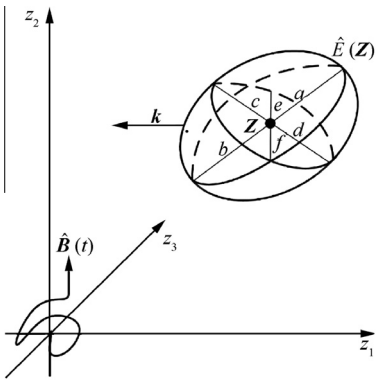

Fig. 5 Transformed coordinates.

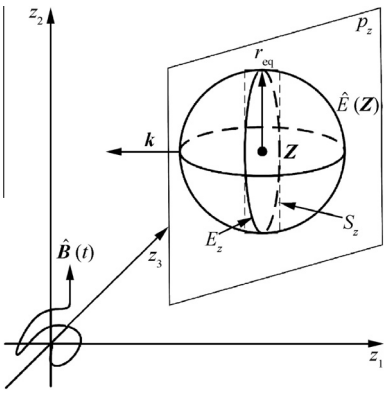

Fig. 6 Region $\hat{E}(\boldsymbol{Z})$ replaced by an equivalent sphere with radius r_{eq}.

domain $\hat{E}(\boldsymbol{Z})$ with an equivalent sphere of radius r_{eq}. An appropriate r_{eq} will make the sphere and the region $\hat{E}(\boldsymbol{Z})$ have the same volume.

Since the safety envelope is composed of four different quarter ellipsoids, the volume of $\hat{E}(\boldsymbol{Z})$ is calculated by

$$V(\hat{E}(\boldsymbol{Z})) = \frac{1}{4}\left(\frac{4\pi ace}{3}+\frac{4\pi ade}{3}+\frac{4\pi bce}{3}+\frac{4\pi bde}{3}\right) \tag{22}$$

The radius of equivalent sphere r_{eq} is given as

$$r_{eq} = \sqrt[3]{\frac{3V(\hat{E}(\boldsymbol{Z}))}{4\pi}} \tag{23}$$

Substituting Eqs. (1) and (22) into Eq. (23), we have

$$r_{eq} = \sqrt[3]{\frac{V_l(V_f V_a + V_f V_d + V_b V_a + V_b V_d)}{4}} \times \tau \tag{24}$$

With the approximation of an equivalent sphere, the matrix $\boldsymbol{M}$ in Eq. (5) becomes

$$\boldsymbol{M} = \mathrm{diag}\left(\frac{1}{r_{eq}^2}, \frac{1}{r_{eq}^2}, \frac{1}{r_{eq}^2}\right) \tag{25}$$

Substituting this expression into Eq. (19), we have

$$\hat{E}(\boldsymbol{Z}) = \{\boldsymbol{Z} \in \mathbf{R}^3 \,|\, \|\boldsymbol{Z} - (\boldsymbol{r} + \boldsymbol{k}t)\| \leqslant r_{eq}\} \tag{26}$$

in the new coordinates (see Fig. 6).

The center of $\hat{E}(\boldsymbol{Z})$ is moving at the constant velocity $\boldsymbol{k}$ starting from position $\boldsymbol{r}$ along the negative z_1 axis direction. An analytical approximation is then presented for the probability in Eq. (18). p_z is defined as the plane that passes through the center $\boldsymbol{Z} = \boldsymbol{r} + \boldsymbol{k}t$ of the sphere $\hat{E}(\boldsymbol{Z})$ at some time instant $t \in [t_0, t_0 + \Delta t]$. Let p_z be orthogonal to the velocity $\boldsymbol{k}$, then p_z divides the sphere $\hat{E}(\boldsymbol{Z})$ into two equal parts. Projecting $\hat{E}(\boldsymbol{Z})$ onto the plane p_z, we obtain a circle E_z with the radius r_{eq}. Define S_z as the minimum bounding square containing the projection circle E_z and S_z has a side length of $2r_{eq}$.

From the previous discussion, we define $p^A(\boldsymbol{X})$ as the probability that space point $\boldsymbol{X}$ enters the safety envelope $E(\boldsymbol{X}^A)$ within $[t_0, t_0 + \Delta t]$, which is transformed as the probability that the Brownian motion $\hat{\boldsymbol{B}}(t)$ starting from the origin hits the sphere $\hat{E}(\boldsymbol{Z})$ whose center moves in the negative z_1 axis direction starting from $\boldsymbol{r}$ at time $t = 0$ s. A conflict occurs if and only if $\hat{\boldsymbol{B}}(t)$ ever wanders into the moving sphere. Since it is difficult to get an analytical expression of such a probability, we approximate it by the probability of the event that, when $\hat{\boldsymbol{B}}(t)$ first hits the moving plane p_z, the impact point is located inside the minimum bounding square S_z.

Usually the velocity $\boldsymbol{k}$ of the sphere $\hat{E}(\boldsymbol{Z})$ is much larger than the variance growth rate of the Brownian motion $\hat{\boldsymbol{B}}(t)$, therefore only the dimension of the sphere perpendicular to $\boldsymbol{k}$ is relevant for the event mentioned above. A similar approximation was used to handle the problem in a two-dimensional case.[11] A formal discussion of the approximation error was reported.[23] Using the minimum bounding square S_z in place of the projected circle E_z to calculate the probability $p^A(\boldsymbol{X})$ contributes to an over approximation and, at the same time, an over estimation of $s(\boldsymbol{X})$.

Define $\lambda := \inf\{t \geqslant 0 \text{ s} \,|\, \hat{\boldsymbol{B}}(t) \in p_z\}$ as the first time that the Brownian motion $\hat{\boldsymbol{B}}(t)$ hits the moving plane p_z. Due to the three coordinates of $\hat{\boldsymbol{B}}(t)$ being independent one-dimensional Brownian motion, λ depends only on the first component $\hat{B}_1(t)$ of $\hat{\boldsymbol{B}}(t)$. Specifically, λ is the first time that the one-dimensional Brownian motion $\hat{B}_1(t)$ starting from the origin hits a point $Z_1(t) \in \mathbf{R}$, which depends on the equation $Z_1(t) = r_1 - \|\boldsymbol{\varphi}\|t$ where r_1 is the first component of $\boldsymbol{r} \in \mathbf{R}^3$.

In the new coordinate system, a negative $r_1 < 0$ indicates that aircraft A is moving away from the space point $\boldsymbol{X}$. That leads to a zero probability of $\boldsymbol{X}$ entering $E(\boldsymbol{X}^A)$. When $r_1 < 0$, we set $p^A(\boldsymbol{X}) = 0$.

When $r_1 \geqslant 0$, the probability distribution of λ is characterized by the probability density function[23]

$$p_\lambda(t) = \frac{r_1}{\sqrt{2\pi t^3}} \mathrm{e}^{-\frac{(r_1 - \|\boldsymbol{\varphi}\|t)^2}{2t}} \quad t \geqslant 0 \text{ s} \tag{27}$$

for any time $T \geqslant 0$ s,

$$\int_0^T p_\lambda(t)\,\mathrm{d}t = 1 - \Phi\left(\frac{r_1 - \|\boldsymbol{\varphi}\|T}{\sqrt{T}}\right) + \mathrm{e}^{2r_1\|\boldsymbol{\varphi}\|}\left[1 - \Phi\left(\frac{r_1 + \|\boldsymbol{\varphi}\|T}{\sqrt{T}}\right)\right] \tag{28}$$

$$\int_0^T t p_\lambda(t)\,\mathrm{d}t = \frac{r_1}{\|\varphi\|}\left\{1 - \Phi\left(\frac{r_1 - \|\varphi\|T}{\sqrt{T}}\right) - \mathrm{e}^{2r_1\|\varphi\|}\left[1 - \Phi\left(\frac{r_1 + \|\varphi\|T}{\sqrt{T}}\right)\right]\right\} \tag{29}$$

where $\Phi(x)=\int_{-\infty}^{x}\frac{1}{\sqrt{2\pi}}e^{-\frac{t^2}{2}}dt$ is the Cumulative Distribution Function (CDF) of a standard normal distribution. We have the relation $\Phi(x)=\frac{1}{2}\left(1+\mathrm{erf}\left(\frac{x}{\sqrt{2}}\right)\right)$ ($\mathrm{erf}(x)$ is the error function $\mathrm{erf}(x)=\frac{2}{\sqrt{\pi}}\int_0^x e^{-t^2}dt$). The time instant $T_h\in[t_0,t_0+\Delta t]$ is the expected time that the Brownian motion $\hat{\boldsymbol{B}}(t)$ hits the plane p_z. It is obtained by

$$T_h=\frac{\int_{t_0}^{t_0+\Delta t}tp_\lambda(t)\,dt}{\int_{t_0}^{t_0+\Delta t}p_\lambda(t)\,dt}=\frac{\int_0^{t_0+\Delta t}tp_\lambda(t)\,dt-\int_0^{t_0}tp_\lambda(t)\,dt}{\int_0^{t_0+\Delta t}p_\lambda(t)\,dt-\int_0^{t_0}p_\lambda(t)\,dt} \tag{30}$$

The projection of the Brownian motion $\hat{\boldsymbol{B}}(t)$ at the impact time λ on the plane p_z is denoted as $\hat{\boldsymbol{B}}_{\mathrm{proj}}(\lambda)\in\mathbf{R}^{2\times2}$. When $\lambda=T_h$, the distribution of $\hat{\boldsymbol{B}}_{\mathrm{proj}}(\lambda)\in\mathbf{R}^{2\times2}$ is a two-dimensional Gaussian random variable with zero mean and covariance $T_h\boldsymbol{I}_2$. The probability density function of $\hat{\boldsymbol{B}}_{\mathrm{proj}}(\lambda)$ is

$$f(x,y)=\frac{1}{2\pi T_h}e^{-\frac{x^2+y^2}{2T_h}} \tag{31}$$

At time $\lambda=T_h$, the probability that $\hat{\boldsymbol{B}}_{\mathrm{proj}}(\lambda)$ is located inside the minimum bounding square S_z is calculated as

$$p(T_h)=P(\hat{\boldsymbol{B}}_{\mathrm{proj}}(\lambda)\in S_z|\lambda=T_h)=\iint_{S_z}f(x,y)\,dx\,dy \tag{32}$$

Defining $\boldsymbol{l}=\boldsymbol{r}+\boldsymbol{k}T_h=[l_1,l_2,l_3]^{\mathrm{T}}$, then the minimum bounding square is obtained by

$$S_z=\{(x,y)\in\mathbf{R}^2|\|x-l_2\|\leqslant r_{\mathrm{eq}},\|y-l_3\|\leqslant r_{\mathrm{eq}}\} \tag{33}$$

From Eqs. (31)–(33), we have

$$\begin{aligned}p(T_h)&=\frac{1}{2\pi T_h}\int_{\|x-l_2\|\leqslant r_{\mathrm{eq}}}e^{-\frac{x^2}{2T_h}}dx\int_{\|y-l_2\|\leqslant r_{\mathrm{eq}}}e^{-\frac{y^2}{2T_h}}dy\\&=\frac{1}{4}\left(\mathrm{erf}(l_2+r_{\mathrm{eq}})-\mathrm{erf}(l_2-r_{\mathrm{eq}})\right)\\&\quad\bullet\left(\mathrm{erf}(l_3+r_{\mathrm{eq}})-\mathrm{erf}(l_3-r_{\mathrm{eq}})\right)\end{aligned} \tag{34}$$

Finally, an approximated expression for $p^A(\boldsymbol{X})$ can be written as

$$\begin{aligned}p^A(\boldsymbol{X})&=\int_{t_0}^{t_0+\Delta t}P(\hat{\boldsymbol{B}}_{\mathrm{proj}}(\lambda)\in S_z|\lambda=T_h)p_\lambda(t)\,dt\\&=p(T_h)\int_{t_0}^{t_0+\Delta t}p_\lambda(t)\,dt\end{aligned} \tag{35}$$

3. Airspace safety field

3.1. Effect of UAV flight performance on conflict probability

From the previous analysis, the safety envelope represents the safe separation requirement between UAVs. As a result of the approximation where we replace the safety envelope $\hat{E}(\boldsymbol{Z})$ with an equivalent sphere in Eq. (21), the equivalent radius r_{eq} can be considered to characterize the safe separation requirement. Reviewing Eq. (24) in Section 2.3,

$$r_{\mathrm{eq}}=\sqrt[3]{\frac{V_l(V_fV_a+V_fV_d+V_bV_a+V_bV_d)}{4}}\times\tau$$

This is rewritten as

$$r_{\mathrm{eq}}=f(\boldsymbol{V})\times\tau \tag{36}$$

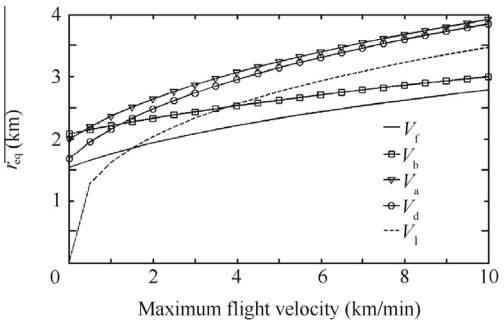

Fig. 7 Variations of r_{eq} with UAV flight performance.

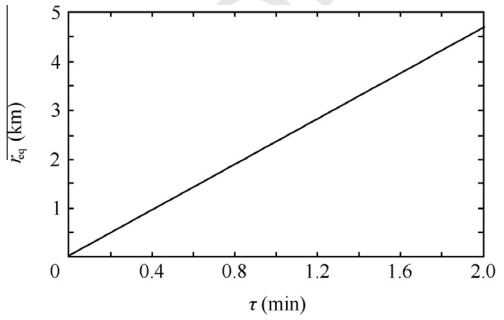

Fig. 8 Variations of r_{eq} with response time τ.

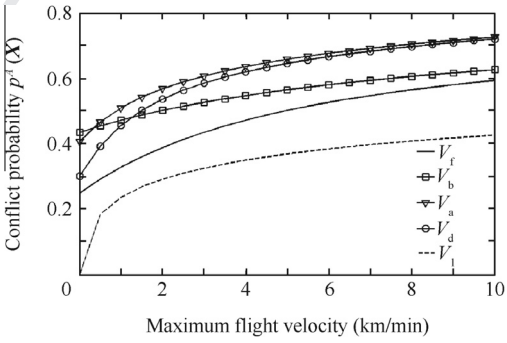

Fig. 9 Variations of conflict probability with UAV flight performance.

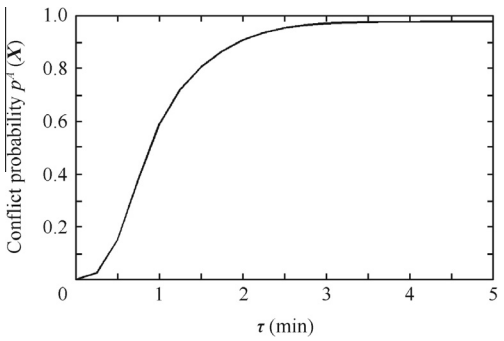

Fig. 10 Variations of conflict probability with response time τ.

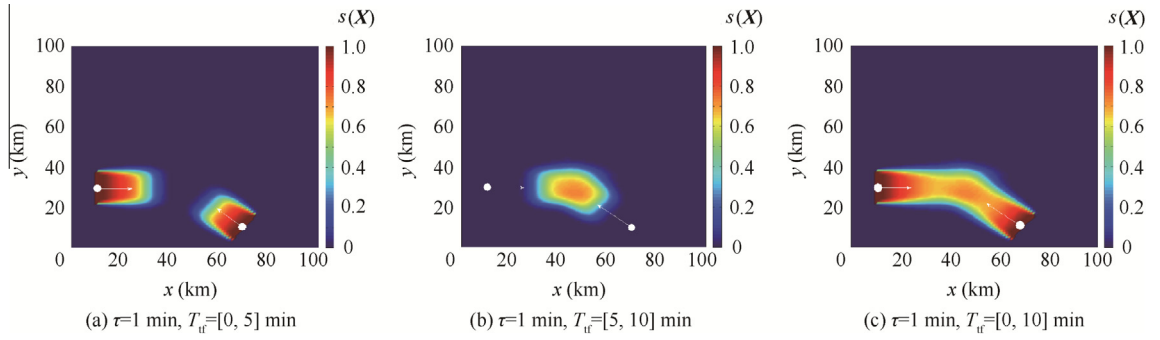

Fig. 11 Airspace safety field in the horizontal plane with response time $\tau = 60$ s.

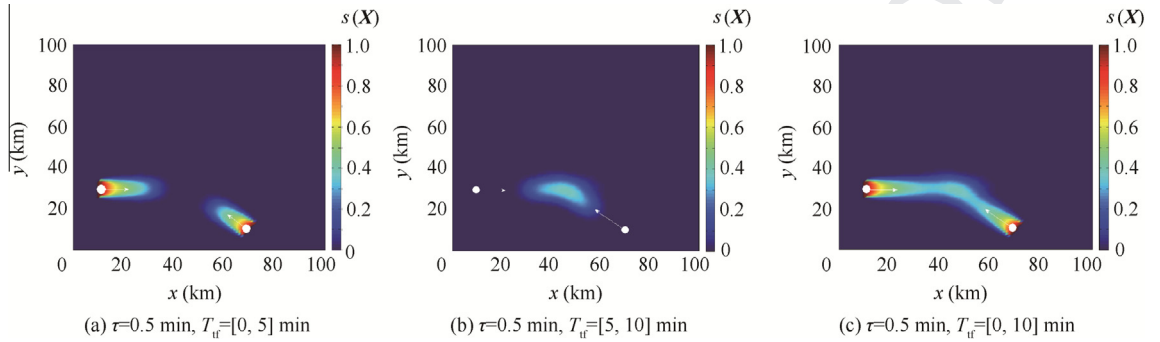

Fig. 12 Airspace safety field in horizontal plane with response time $\tau = 30$ s.

where $\boldsymbol{V} = [V_\mathrm{f}, V_\mathrm{b}, V_\mathrm{a}, V_\mathrm{d}, V_\mathrm{l}]^\mathrm{T}$ is the state vector of UAV flight performance. For example, consider UAV A moves at a velocity $v^A = [5, 0, 0]^\mathrm{T}$ km/min from $\boldsymbol{X}^A = [20, 40, 0]^\mathrm{T}$ km in the time frame $[t_0, t_0 + \Delta t] = [0, 10]$ min. The UAV's maximum flight velocities are given as follows: $V_\mathrm{f}^* = 5$ km/min, $V_\mathrm{b}^* = 2$ km/min, $V_\mathrm{a}^* = 0.9$ km/min, $V_\mathrm{d}^* = 1.5$ km/min, $V_\mathrm{l}^* = 3$ km/min; the response time is given as $\tau^* = 60$ s. Then we have the reference state $\boldsymbol{V}^* = [V_\mathrm{f}^*, V_\mathrm{b}^*, V_\mathrm{a}^*, V_\mathrm{d}^*, V_\mathrm{l}^*]^\mathrm{T}$ and the reference $r_\mathrm{eq}^* = 2.33$ km. Around the reference state, the effect of the maximum forward velocity V_f on r_eq can be formulated as

$$r_\mathrm{eq} = \sqrt[3]{\frac{V_\mathrm{l}^*[(V_\mathrm{a}^* + V_\mathrm{d}^*)V_\mathrm{f} + V_\mathrm{b}^* V_\mathrm{a}^* + V_\mathrm{b}^* V_\mathrm{d}^*]}{4}} \times \tau^* \tag{37}$$

In this way, the similar relations between r_eq and $V_\mathrm{b}, V_\mathrm{a}, V_\mathrm{d}, V_\mathrm{l}, \tau$ can be derived.

In Fig. 7, r_eq grows when maximum flight velocity increases in any direction, although the growth rates are different. Fig. 8 shows r_eq performing a linear growth with response time.

Using first order approximation of Taylor expansion to expand Eq. (37) around the reference state $\boldsymbol{V}^* = [V_\mathrm{f}^*, V_\mathrm{b}^*, V_\mathrm{a}^*, V_\mathrm{d}^*, V_\mathrm{l}^*]^\mathrm{T}$ and $\tau^* = 60$ s, we have

$$\begin{aligned} r_\mathrm{eq} = r_\mathrm{eq}^* &+ \left.\frac{\partial r_\mathrm{eq}}{\partial V_\mathrm{f}}\right|_{V^*,\tau^*} \times \Delta V_\mathrm{f} + \left.\frac{\partial r_\mathrm{eq}}{\partial V_\mathrm{b}}\right|_{V^*,\tau^*} \times \Delta V_\mathrm{b} + \left.\frac{\partial r_\mathrm{eq}}{\partial V_\mathrm{a}}\right|_{V^*,\tau^*} \\ &\times \Delta V_\mathrm{a} + \left.\frac{\partial r_\mathrm{eq}}{\partial V_\mathrm{d}}\right|_{V^*,\tau^*} \times \Delta V_\mathrm{d} + \left.\frac{\partial r_\mathrm{eq}}{\partial V_\mathrm{l}}\right|_{V^*,\tau^*} \times \Delta V_\mathrm{l} + \left.\frac{\partial r_\mathrm{eq}}{\partial \tau}\right|_{V^*,\tau^*} \\ &\times \Delta\tau \end{aligned} \tag{38}$$

Define $\Delta V_i = V_i - V_i^* \quad (i = \mathrm{f}, \mathrm{b}, \mathrm{a}, \mathrm{d}, \mathrm{l})$, $\Delta\tau = \tau - \tau^*$, and $\Delta r_\mathrm{eq} = r_\mathrm{eq} - r_\mathrm{eq}^*$. Substituting the reference state into Eq. (38), we have

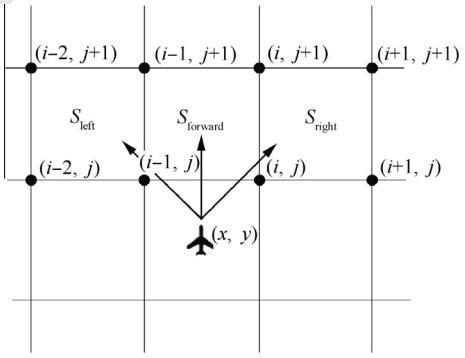

Fig. 13 UAV conflict resolution in horizontal plane.

$$\begin{aligned} \Delta r_\mathrm{eq} = {} & 0.11\Delta V_\mathrm{f} + 0.11\Delta V_\mathrm{b} + 0.32\Delta V_\mathrm{a} + 0.32\Delta V_\mathrm{d} \\ & + 0.26\Delta V_\mathrm{l} + 2.33\Delta\tau \end{aligned} \tag{39}$$

Because of the bilateral symmetry of UAV flight performance, r_eq has the same variation rate in the plane of symmetry, such that

$$\left.\frac{\partial r_\mathrm{eq}}{\partial V_\mathrm{f}}\right|_{V^*,\tau^*} = \left.\frac{\partial r_\mathrm{eq}}{\partial V_\mathrm{b}}\right|_{V^*,\tau^*} = 0.11$$

But, they are different in the plane of asymmetry. Generally, the velocities of a UAV in the horizontal plane are faster than those in the vertical plane. r_eq is more sensitive to changes in vertical velocity. Hence,

$$\left.\frac{\partial r_\mathrm{eq}}{\partial V_\mathrm{a}}\right|_{V^*,\tau^*} > \left.\frac{\partial r_\mathrm{eq}}{\partial V_\mathrm{f}}\right|_{V^*,\tau^*}, \quad \left.\frac{\partial r_\mathrm{eq}}{\partial V_\mathrm{a}}\right|_{V^*,\tau^*} > \left.\frac{\partial r_\mathrm{eq}}{\partial V_\mathrm{l}}\right|_{V^*,\tau^*}$$

In order to analyze the effect of UAV flight performance on conflict probability, considering a space point $\boldsymbol{X} = [55, 35, 0]^{\mathrm{T}}$ km, we obtain the conflict probability between UAV A and point $\boldsymbol{X}$ (see Fig. 9).

Apparently, the conflict probability increases with maximum flight velocity in each direction. This is because the increase of maximum flight velocity enlarges the integral domain when calculating the conflict probability.

From Eq. (36), r_{eq} is of a linear growth rate with the response time τ around the reference state $\boldsymbol{V}^*$. The conflict probability also significantly increases with the response time τ. When $\tau = 3$ min, the safety envelope grows to three times that which would result in a certain conflict between UAV A and point $\boldsymbol{X}$. The conflict probability $p^A(\boldsymbol{X}) \approx 1.0$ (see Fig. 10).

Taking the effect of UAV flight performance into consideration when determining safe separation will improve the utilization efficiency of airspace. According to Eq. (36), the safety envelope is variable for different UAVs and different response times.

3.2. Construction of airspace safety field

Supposing there are n UAVs existing in the airspace, we obtain the measure of airspace safety

$$s(\boldsymbol{X}) = f(n, t_0, \Delta t, \boldsymbol{X}, \boldsymbol{X}_0^i, \boldsymbol{v}^i, \sum^i, V_{\mathrm{f}}^i, V_{\mathrm{b}}^i, V_{\mathrm{a}}^i, V_{\mathrm{d}}^i, V_{\mathrm{l}}^i, \tau^i) \quad i = 1, 2, \ldots, n \tag{40}$$

If the parameters mentioned above are obtained, $s(\boldsymbol{X})$ is determined. The increase of V_{f}, V_{b}, V_{a}, V_{d}, V_{l} and τ will result in a larger safety envelope and also a larger integral domain when computing the conflict probability $p^A(\boldsymbol{X})$. In Eq. (8), $s(\boldsymbol{X})$ is obviously an increasing function of $p^A(\boldsymbol{X})$. If $\boldsymbol{X}$ varies over S, an airspace safety field can be constructed. Discretizing airspace $\boldsymbol{S}$ by using a uniform gridding of step size $\rho > 0$ along all axes, one can evaluate $s(\boldsymbol{X})$ across $\boldsymbol{S}$. The following examples are for illustration.

Fig. 11(a)–(c) are the airspace safety fields in the horizontal plane during different time frames T_{tf}. In the simulation, two UAVs move in the horizontal plane at the same constant velocity $v = 4$ km/min. They also have the same flight performance, with the maximum velocities given in Section 3.1. One UAV moves to east while the other moves northwest (the white dots and arrows denote the positions and directions of UAVs). Models of the safety field during three time frames $[0, 5]$ min, $[5, 10]$ min and $[0, 10]$ min are shown. In Fig. 11, the red[1] areas indicate the occupied region of a certain existing UAV, hence new entered UAVs should avoid passing through this area within the time frame T_{tf}. The blue area represents the free region of no existing UAVs. An intermediate color between red and blue signifies the degree of danger according to the magnitude of probability. In Fig. 12, the response time is half of that in Fig. 11, with a corresponding halving in size of the safety envelope. A smaller safety envelope means a smaller protected zone to avoid being penetrated. Therefore, the congested area of high conflict risk in Fig. 12 is less than that of Fig. 11. This is apparently observed in the airspace safety field.

The airspace safety field clearly shows the occupancy distribution of airspace. Constructing the safety fields for different consecutive time intervals can predict when UAVs enter and leave a certain zone in the airspace. This information can be used for detecting congested areas within time-space coordinates. The availability of airspace safety field can support UAV conflict resolution and trajectory planning.

4. Applications of airspace safety fields

4.1. Conflict resolution

The airspace safety field is composed of the conflict probability in each discrete point after the airspace was discretized. When airspace safety conditions around a UAV in the future time interval $[0, t]$ is obtained, UAV conflict resolution can be performed. Usually, there are four kinds of maneuvering for UAV flight conflicts: left turn or right turn in the horizontal plane and climbing or descending in vertical plane. In Fig. 13,

(a) Artificial poles

(b) Experimental UAV

Fig. 14 Experiment site.

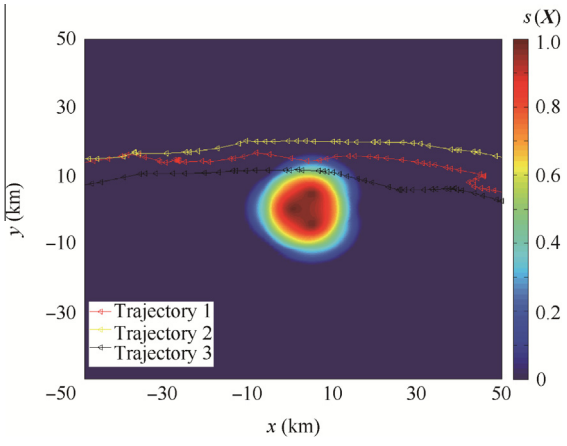

Fig. 15 Trajectories of three UAVs.

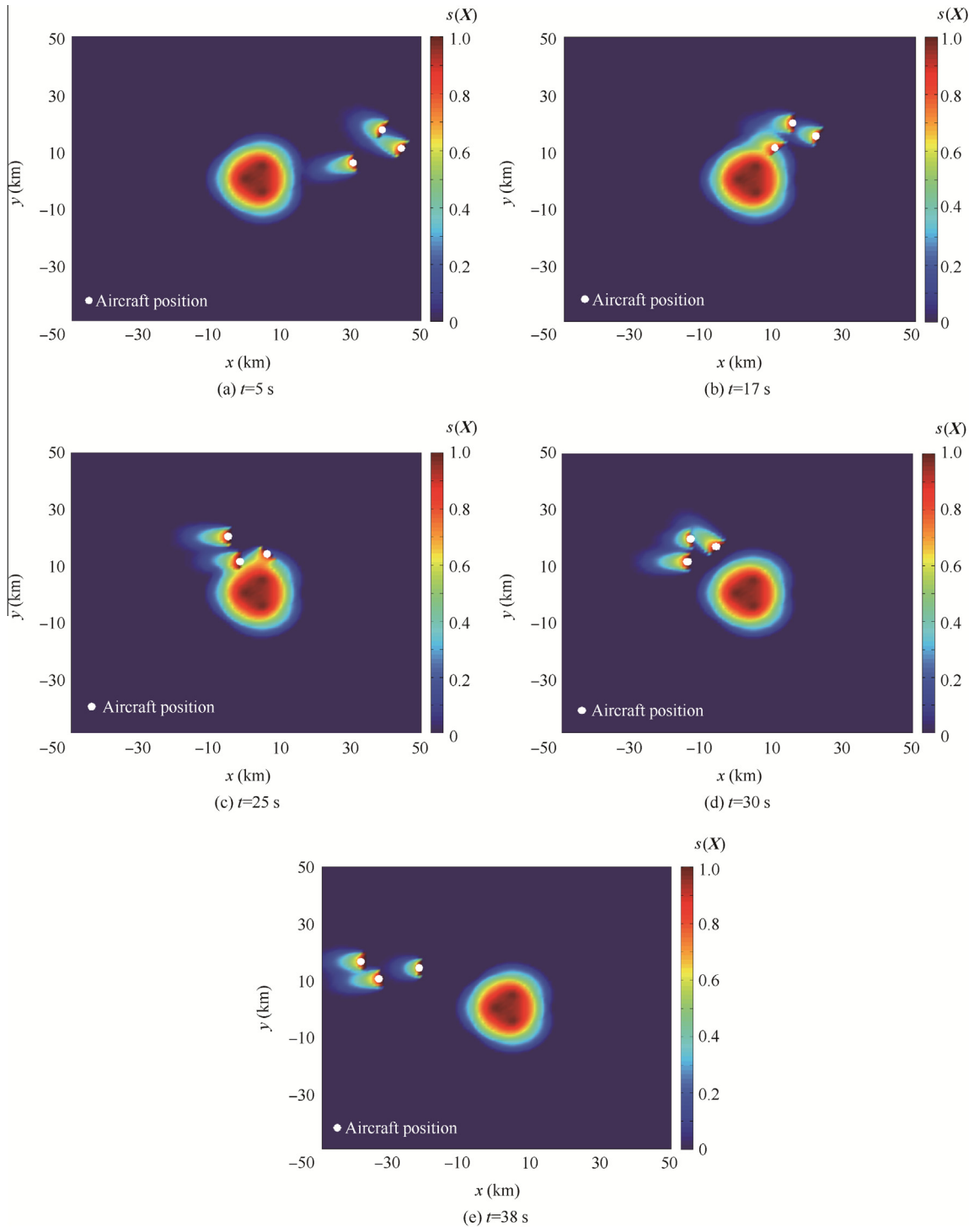

Fig. 16 Variations of safety fields in formation flight.

take the safety of the horizontal plane as an example. Suppose a UAV is flying at a constant velocity, and $\boldsymbol{X} = [x, y]^T$ is the UAV's current position. $i = \min\{\tilde{x} \in \mathbf{Z} | \tilde{x} \geqslant x\}$, $j = \min\{\tilde{y} \in \mathbf{Z} | \tilde{y} \geqslant y\}$, $(\mathbf{Z})$ is the set of integers. The conflict probability $p(\boldsymbol{X}_{i,j})$ indicates the safety of point $\boldsymbol{X}_{i,j}$ and can be calculated by Eq. (35). Denote S_{forward} as the unit area in front of the UAV. Similarly, S_{left} is the front-left unit area of the UAV and S_{right} is the front-right unit area of the UAV (see Fig. 13). If $p(S_{\text{forward}})$ is the conflict probability of the unit area in front of the UAV, we have

$$p(S_{\text{forward}}) = \frac{1}{4}\left(p(\boldsymbol{X}_{i-1,j}) + p(\boldsymbol{X}_{i,j}) + p(\boldsymbol{X}_{i-1,j+1}) + p(\boldsymbol{X}_{i,j+1})\right) \quad (41)$$

In the same way, we have

$$p(S_{\text{left}}) = \frac{1}{4}\left(p(\boldsymbol{X}_{i-2,j}) + p(\boldsymbol{X}_{i-1,j}) + p(\boldsymbol{X}_{i-2,j+1}) + p(\boldsymbol{X}_{i-1,j+1})\right) \quad (42)$$

$$p(S_{\text{right}}) = \frac{1}{4}\left(p(\boldsymbol{X}_{i,j}) + p(\boldsymbol{X}_{i+1,j}) + p(\boldsymbol{X}_{i,j+1}) + p(\boldsymbol{X}_{i+1,j+1})\right) \quad (43)$$

Define p_0 as the threshold of conflict probability. If $p(S_{\text{forward}}) < p_0$, the UAV maintains forward flight. If $p(S_{\text{forward}}) \geqslant p_0$, a conflict alert is given. Comparing $p(S_{\text{left}})$ and $p(S_{\text{right}})$, if $p(S_{\text{left}}) < p(S_{\text{right}})$, the UAV changes heading and performs a left-turn maneuver, otherwise it performs a right-turn maneuver.

The same principle applies in a three-dimensional case. Define S_{above} as the front-above unit area of the UAV and S_{below} as the front-below unit area of the UAV. When a conflict occurs, maneuvering in horizontal plane is considered preferable. If $p(S_{\text{forward}}) \geqslant p_0$, $p(S_{\text{left}}) \geqslant p_0$ and $p(S_{\text{right}}) \geqslant p_0$, it means the conflict cannot be solved in the horizontal plane. Comparing $p(S_{\text{above}})$ and $p(S_{\text{below}})$, if $p(S_{\text{above}}) < p(S_{\text{below}})$, the UAV performs a climbing maneuver, otherwise it performs a descending maneuver.

To illustrate the validity of airspace safety construction and the conflict resolution method, an experiment of UAV formation flying with obstacle avoidance is performed. Since power lines and towers are some of the most dangerous obstacles in low altitude airspace, a dried-up riverbed is chosen as the experiment site. We constructed three artificial poles in a triangle and joined the three peaks with power lines to simulate obstacles (see Fig. 14).

Fig. 15 shows the trajectories that UAVs use to avoid the artificial obstacle. Three UAVs fly from east to west in the horizontal plane with the altitude $H = 15$ m. The red area in the center of Fig. 18 indicates the addition of the artificial poles into the safety field.

Fig. 16 illustrates the variations of safety fields in formation flight. UAVs take off at time $t = 0$ s. Five different moments at 5, 17, 25, 30 and 38 s are chosen to determine the safety field. The time variants and tendencies of the safety field can easily be observed. The heading changes made by UAVs when performing conflict resolution can also be observed.

4.2. Trajectory planning

Consider that UAV B enters the airspace region S where other UAVs are flying. UAV B starts from the entry point at time 0 to the destination before time T at a constant velocity. The predetermined trajectory of UAV B is a straight line. However, as a result of the presence of other UAVs, this trajectory is not ensured to be of low conflict risk. UAV B can pick a fixed number m of direction changes at specified points in time $0 < t_1 < t_2 < \cdots < t_m < t$.

The problem of finding an optimal trajectory that minimizes the sum of the total flight time and the conflict risk along its current trajectory is formulated as

$$\begin{aligned} &J = \min\left\{T_n + \eta \int_0^z s(\boldsymbol{X})\,\mathrm{d}\boldsymbol{X}\right\} \\ &\text{s.t. } T_n = \frac{d_n}{\|\boldsymbol{v}^B\|}, \quad t \in [t_0, t_0 + \Delta t] \end{aligned} \quad (44)$$

where J is a weighted sum of the total flight time T_n and the conflict risk along its trajectory; z is the trajectory of UAV B; d_n is the total distance of the trajectory; $\boldsymbol{v}^B$ is the velocity of UAV B and η is the weight coefficient. The first term of cost function J shows the economic requirement that UAV B needs to fly through the airspace as quickly as possible. The second term represents the safety requirement that the conflict risk along the trajectory must be as low as possible.

In the computation of $s(\boldsymbol{X})$, the trajectory is discretized by m waypoints. Therefore, the sum of the conflict risk of the waypoints $\boldsymbol{p}_1, \boldsymbol{p}_2, \ldots, \boldsymbol{p}_m$ is taken as a measure of the conflict risk along its trajectory. The cost function J reduces to

$$J = \min\left\{T_n + \eta \sum_{i=1}^{m} s(\boldsymbol{p}_i)\right\} \quad (45)$$

This problem can be easily solved by the sequential quadratic programming (SQP) method, which has proven highly effective for solving constrained optimization problems with smooth nonlinear functions in the objectives and constraints.[24] In this example, the predetermined straight trajectory is taken as the initial condition for the solution. Because the velocity of UAV B is constant, a smaller η means the less deviation of

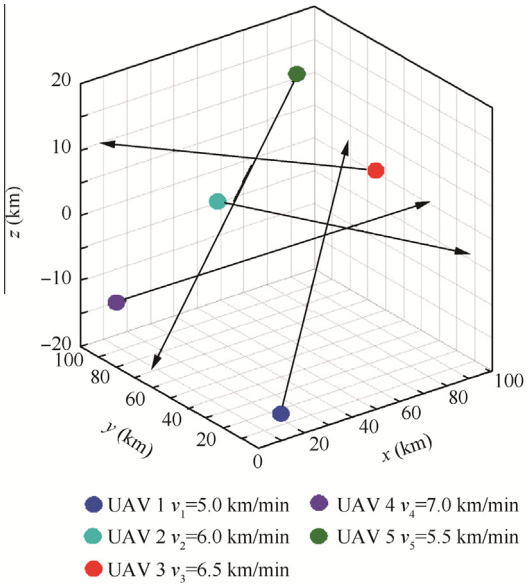

Fig. 17 Nominal trajectories and velocities of five UAVs.

Table 1 Parameters used in example.

Parameter	Value
σ_1^A (km (min)$^{-1/2}$)	0.2
σ_2^A (km (min)$^{-1/2}$)	0.1
σ_3^A (km (min)$^{-1/2}$)	0.1
V_{f} (km/min)	5
V_{b} (km/min)	2
V_{a} (km/min)	0.9
V_{d} (km/min)	1.5
V_{l} (km/min)	3
τ (s)	60
T (min)	15
$\boldsymbol{v}^B$ (km/min)	$[0, 10, 0]^{\text{T}}$
$\boldsymbol{X}_0$ (km)	$[50, 0, H]^{\text{T}}$
$\boldsymbol{X}_{\text{D}}$ (km)	$[50, 100, H]^{\text{T}}$
m	99

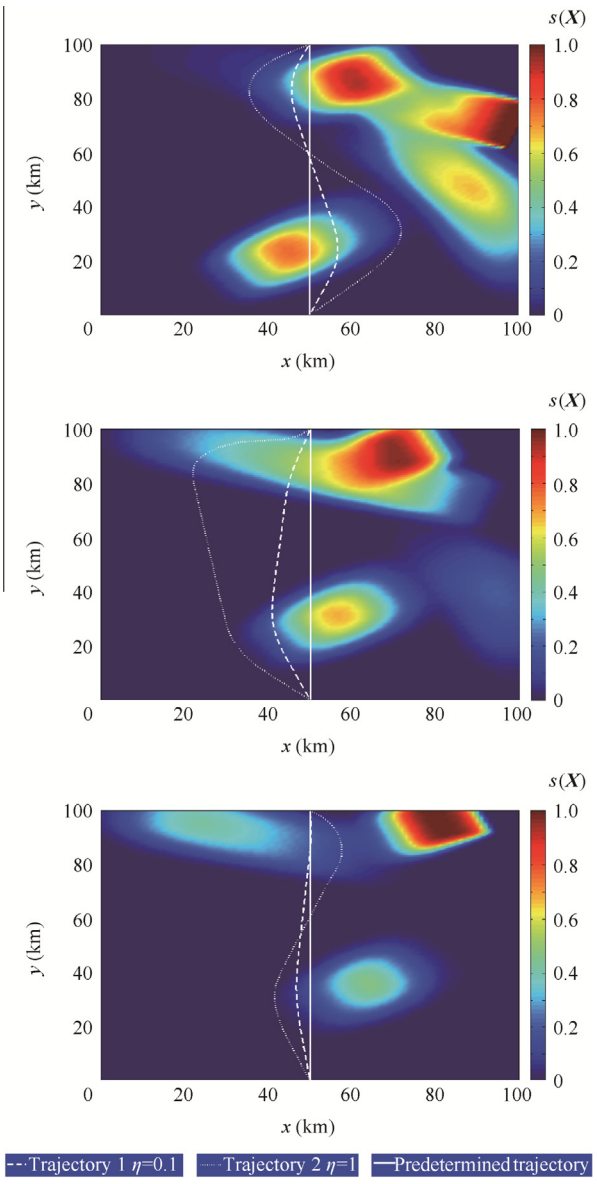

Fig. 18 Safety field and optimal trajectories in horizontal plane.

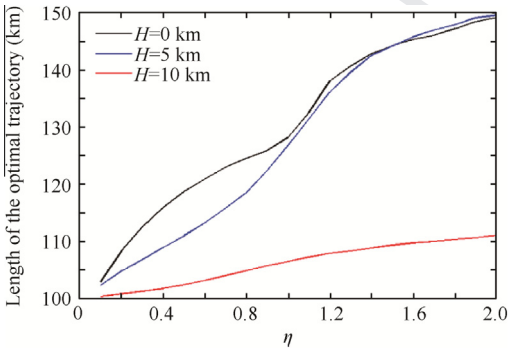

Fig. 19 Length of optimal trajectory of 0, 5 and 10 km high planes.

predetermined trajectory and less flight time. A bigger η contributes a greater priority to the low conflict risk requirement and leads to a less conflict-prone trajectory for safety.

Supposing that five UAVs are moving in a three-dimensional airspace region and each UAV is flying at constant velocity along a straight line during the time interval T. The nominal trajectories of UAVs are shown in Fig. 17.

The uncertainty that affects UAV future positions is characterized by σ_1^A, σ_2^A and σ_3^A. The number of waypoints is taken as $m = 99$ (e start point and the end point are not included). UAV B has to fly through the airspace region in 15 min at a constant velocity. The entry point and destination point of UAV B are $\boldsymbol{X}_0$ and $\boldsymbol{X}_D$. UAV B can change its direction only on the horizontal plane. All the parameters used in the example are given in Table 1.

Fig. 18(a) shows the airspace safety field and optimal trajectory of UAV B on the horizontal plane of $H = 0$ km high. When UAV B needs to go through the airspace region as soon as possible, trajectory 1 will be optimal, but this trajectory is at risk for conflict with other UAVs. In contrast, trajectory 2 is more safe, although it takes more time. However, there is a tradeoff between efficiency and safety that depends on the choice of appropriate weight coefficient η. Fig. 18(b) and (c) show the cases of $H = 5$ km high and $H = 10$ km high, respectively.

Fig. 19 shows that the length of all three optimal trajectories increase when the weight coefficient η grows. Obviously, the higher η denotes greater safety requirements and leads to a longer trajectory. UAVs need to avoid approaching the congested regions of high conflict risk, which results in more deviation in predetermined trajectory.

5. Conclusions

(1) The safety envelope is a variable-size protected zone for different UAVs. In a predetermined response time, the conflict probability increases with the maximum flight velocity of UAV in each direction.

(2) Based on the uncertainty of UAV positions in the future, a probabilistic approach is presented to evaluate the conflict probability between a space point and the UAV safety envelope in a mid-term horizon. With the assumption of equivalent spheres, an analytical approximation of the conflict probability is derived.

(3) The airspace safety field is constructed to indicate the occupancy distribution of airspace. This information can be used for UAV conflict resolution and trajectory planning of newly entering UAVs.

Acknowledgement

This work was supported by the National Basic Research Program of China (No. 2011CB707002).

References

1. Zhang J. New development and application of airspace surveillance technology. *Acta Aeronaut Astronaut Sin* 2011;**32**(1):1–14 [Chinese].
2. Reich PG. Analysis of long-range air traffic systems: separation standards I. *J Navigation* 1966;**19**(1):88–98.
3. Reich PG. Analysis of long-range air traffic systems: separation standards II. *J Navigation* 1966;**19**(2):169–86.
4. Reich PG. Analysis of long-range air traffic systems: separation standards III. *J Navigation* 1966;**19**(3):331–47.

5. Brooker P. Lateral collision risk in air traffic system: a 'Post—REICH' event model. *J Navigation* 2003;**56**(3):399–409.
6. Kopardekar P, Schwartz A, Magyarits S, Rhodes J. Airspace complexity measurement: an air traffic control simulation analysis. *Int J Indust Eng-Theory Appl Pract* 2009;**16**(1):61–70.
7. Sridhar B, Sheth KS, Grabbe S. Airspace complexity and its application in air traffic management*Proceedings of the 2nd USA/Europe air traffic management R&D semina, 1998 December 1–4*. Orlando (FL), Brussels (Belgium): Eurocontrol Press; 1999.
8. Prandini M, Putta V, Hu JH. A probabilistic measure of air traffic complexity in 3-D airspace. *Int J Adapt Control Sig Process* 2010;**24**(10):813–29.
9. Paielli RA, Erzberger H. Conflict probability estimation for free flight. *J Guid Control Dyn* 1997;**20**(3):588–96.
10. Yang LC, Kuchar JK. Prototype conflict alerting system for free flight. *J Guid Control Dyn* 1997;**20**(4):768–73.
11. Prandini M, Hu JH, Lygeros J, Sastry S. A probabilistic approach to aircraft conflict detection. *IEEE Trans Intell Transport Syst, Spec Iss Air Traffic Control - Part I* 2000;**1**(4):199–220.
12. Hu JH, Prandini M, Sastry S. Aircraft conflict prediction in the presence of a spatially correlated wind field. *IEEE Trans Intell Transport Syst* 2005;**16**(3):326–40.
13. Jackson JA, Boskovic JD. Application of airspace encounter model for prediction of intruder dynamics*AIAA modeling and simulation technologies conference, 2012 August 13-16*. Minneapolis (MN), Reston: AIAA; 2012. p. 985–1004.
14. Blom HAP, Bakker GJ. Conflict probability and incrossing probability in air traffic management*Proceedings of the 41st IEEE conference on decision and control, 2002 December 10–13*. Las Vegas (NV), Piscataway (NJ): IEEE Press; 2003. p. 2421–6.
15. Blom HAP, Krystul J, Bakker GJ, Klompstra MB, Klein Obbink BK. Free flight collision risk estimation by sequential Monte Carlo simulation*Stochastic hybrid systems*. Taylor & Francis/CRC Press; 2007. p. 249–81.
16. Visintini AL, Glover W, Lygeros J, Maciejowski J. Monte Carlo optimization for conflict resolution in air traffic control. *IEEE Trans Intell Transport Syst* 2006;**7**(4):470–82.
17. Lygeros J. On reachability and minimum cost optimal control. *Automatica* 2004;**40**(6):917–27.
18. Mitchell I, Bayen A, Tomlin C. A time-dependent Hamilton-Jacobi formulation of reachable sets for continuous dynamic games. *IEEE Trans Autom Control* 2005;**50**(7):947–57.
19. Gillula JH, Huang HM, Vitus MP, Tomlin CJ. Design of guaranteed safe maneuvers using reachable sets: autonomous quadrotor aerobatics in theory and practice. In: Proceedings of 2010 IEEE international conference on robotics and automation, 2010 May 3–8. Anchorage (AK), Piscataway (NJ): IEEE Press; 2010. p. 1649–54.
20. Greatwood C, Richards A. Minimal sensor scanning volumes for helicopter terrain avoidance. In: AIAA guidance, navigation and control conference, 2010 August 2–5. Toronto. Reston: AIAA; 2010. p. 1–8.
21. Nanjian Z, Zhangping L, Yiru R, Jinwu X. Fast calculation method for helicopter reachable domain in forward flight. *J Beijing Univ Aeronaut Astronaut* 2014;**40**(6):810–4 [Chinese].
22. Erzberger H, Paielli RA, Isaacson DR, Eshow MM. Conflict detection and resolution in the presence of prediction error. In: Proceedings of the 1st USA/Europe air traffic management R&D seminar, 1997 June 17–20. Saday (France), Brussels (Belgium): Eurocontrol Press; 1997.
23. Hu JH. *A study of conflict detection and resolution in free flight* [dissertation]. Berkeley: University of California at Berkeley; 1999.
24. Gill PE, Murray W, Saunders MA. SNOPT: an SQP algorithm for large-scale constrained optimization. *SIAM J Optimiz* 2006;**12**(4):979–1006.

Xiang Jinwu is a professor and Ph.D. supervisor at the School of Aeronautic Science and Engineering, Beihang University, Beijing, China. He received his Ph.D. from Nanjing University of Aeronautics and Astronautics in 1993. His current research interests include UAV systems, aircraft dynamics and control.

Liu Yang is a Ph.D. student at the School of Aeronautic Science and Engineering, Beihang University, Beijing, China. His areas of research include aircraft trajectory optimization and conflict detection and resolution.

Luo Zhangping is an associate professor and master student supervisor at the School of Aeronautic Science and Engineering, Beihang University, Beijing, China. He received his Ph.D. from Beihang University in 2004. His current research interests include flight safety, aircraft dynamics and control.

Please cite this article in press as: Jinwu X et al. Flight safety measurements of UAVs in congested airspace, *Chin J Aeronaut* (2016), http://dx.doi.org/10.1016/j.cja.2016.08.017